Erschienen in: Journal of Materials Chemistry B ; 6 (2018), 5. - S. 816-823
https://dx.doi.org/10.1039/c7tb01790a

Optical glucose sensing using ethanolamine–polyborate complexes†

C. Toncelli, *[a] R. Innocenti Malini, [a] D. Jankowska, [b] F. Spano,[a] H. Cölfen, [c] K. Maniura-Weber, [b] R. M. Rossi[a] and L. F. Boesel *[a]

Wound monitoring is essential to tackle chronic complications at their infancy and thus objectively scrutinize any delay in the epithelization process. Since glucose in wound exudates is recognized as key bio-marker in wound monitoring, the development of a cost-efficient detection method for glucose would aid at tackling early-stage infections in wounds. For the first time, we present a novel platform for one-step synthesis of non-enzymatic, cost-efficient optical glucose sensors. These are based on complexes formed by the interactions between polyborates and ethanolamines. The complexes, synthesized by just heating a solution of boric acid and ethanolamines at 150 °C, were characterized using ^{13}C-NMR, ^{1}H-NMR, ^{11}B-NMR, analytical ultracentrifugation and DFT. The results show that the complexes in solution are extremely small (hydrodynamic diameter of around 0.5 nm) and that the polyborates species interact with the ethanolamines *via* both moderate and weak hydrogen bondings. These complexes were then tested on glucose concentrations ranging from 0 to 10 mM, showing significant changes in the fluorescent emission between the glucose level expressed in an healable wound (5.0–7.6 mM) and a chronic one (0.3–1.0 mM).

Introduction

Boron compounds are often utilized as molecular building blocks to guide the assembly of hierarchical structures due to their versatile chemistry. Thanks to the presence of boron as light-weight element, their porosity, density and thermal stability outperforms their metallic-based counterparts.[1,2]

Such multi-facet advantages lead to potential applications in hydrogen storage,[3] filtration,[4] catalysis[5] and optoelectronics.[6]

Boronate esterification, Lewis base coordination and boroxine formation (*i.e.* condensation of the boronic acid to yield a partly aromatic six-membered B–O–B structure), hydrogen bonding and spiroborate formation[7] represent only a glimpse in the synthetic pathways that helps to define at a molecular scale boron-based covalent organic frameworks (COFs).

The molecular architecture can also be steered by the addition of other conjugation strategies, such as triazine moieties from aromatic nitriles, Schiff base chemistry and imide condensation reactions.[8]

The main bottleneck of such structures is the inherent poor hydrolytic stability of boronic ester and boroxine rings chemical groups,[9,10] which strongly confines their viability to humidity-controlled or water-free environments.

To overcome this limiting factor, enhanced hydrostability have been shown when COF-5 (2,3,6,7,10,11-hexahydroxytriphenylene and benzene-1,4-diboronic acid as precursors) and COF-10 (2,3,6,7,10,11-hexahydroxytriphenylene and 4,4′-biphenyldiboronic acid as precursors) are reacted with pyridine to induce a dative bond between the boron and the nitrogen atom.[9] However, such stabilization is absent when COF-1 (obtained by condensation reaction of benzene-1,4-diboronic acid) is employed.[10] The hypothesized reason behind such discrepancy is that only the B-COF frameworks containing weakly acidic B·O(H)·C defect sites can be stabilized by forming a Brønsted-type interaction with the N-donors.[11]

Boric acid, if compared to the boronic acids employed in COFs, shows specular reactivities with condensation routes forming metaboric acid and fused boroxole rings, as well as boronic ester linkages.

As already mentioned in the case of COFs, polyborates composed of fused boroxole rings with 3, 4, 5, 6, 7 and/or 9 boron atoms were synthesized at temperatures higher than 130 °C[12] by stabilizing their structures thanks to the presence of an amine ligands.

[a] *Empa, Swiss Federal Laboratories for Materials Science and Technology, Laboratory for Biomimetic Membranes and Textiles, Lerchenfeldstrasse 5, CH-9014 St. Gallen, Switzerland. E-mail: claudio.toncelli@empa.ch, luciano.boesel@empa.ch*
[b] *Empa, Swiss Federal Laboratories for Materials Science and Technology, Biointerfaces, Lerchenfeldstrasse 5, CH-9014 St. Gallen, Switzerland*
[c] *Max-Planck-Institut für Kolloid – und Grenzflächenforschung, Kolloidchemie, Forschungscampus Golm, 14424 Potsdam, Germany*

† Electronic supplementary information (ESI) available. See DOI: 10.1039/c7tb01790a

Interestingly, the formation of such complex, whose size is comparable to conventional organic fluorophores, lead to a partially delocalized aromatic structure where exciton decay occurs *via* a fluorescent radiative process.[13–16]

Indeed, it has already been observed that complex formation between boric acid and isopropyltrimethylammonium hydroxide led to the synthesis of a fluorescent polyborate composed of pentaborate salts stabilized by amine ligands.[16]

These set of complexes retain their fluorescence even in aqueous solutions and display a carbon dot-like excitation-dependent emission.[17,18]

Synthesis of fluorophores directly connected with boronate receptors have been shown to alter their photoluminescent emission as a consequence of reversible cross-linking with 1,2-diols.[19] Similar approaches which utilize diffracted light as transducing element integrate the use of photonic crystals within a hydrogel displaying phenylboronic units for glucose monitoring in tear fluid.[20] As a result, non-enzymatic glucose sensors were fabricated by following this route. Unfortunately, such sensor chemistry is not selective towards glucose, as it targets all the mono- and poly-saccharides eventually present in the analyte matrix.

Even though this issue has been partly tackled by engineering the design of the borate receptor, the derived structures rely on laborious and time-consuming synthesis pathways, which drastically hamper their up-scaling in view of commercial applications.

Hence, there is a compelling need of a facile synthetic platform for the development of optical glucose sensors with remarkable selectivity.

Hereby, we present polyborate–amine complexes as a novel optical platform for glucose detection. We have employed boric acid and ethanolamine as binary precursors, with the latter being both co-reactant and reaction medium. This one-pot reaction, that requires relatively mild temperatures (*i.e.* 150 °C), cost-effective precursors and simple laboratory set-up viable for up-scaling to industrial needs, is certainly appealing for the development of non-enzymatic optical glucose sensors.

These sensors were then tested to detect glucose as bio-marker for the assessment of the wound status. The results showed that the developed sensor can reliably discriminate between glucose concentrations related to healable and chronic wounds, thus offering a promising alternative to the previous state of the art in non-enzymatic based sensors. They may also replace enzymatic glucose sensors for wound monitoring,[21] with advantages in terms of stability and simplicity of the system.

Results and discussion

Synthesis and characterization of polyborates/MEA complexes

The reaction between ethanolamine and boric acid was carried out by heating up the mixture at a temperature of 150 °C for 230 minutes. The reaction time was optimized *via* a kinetic monitoring using fluorescence spectroscopy (Fig. S-1, ESI†). The reaction temperature was set at an intermediate value between the boiling point of ethanolamine (170 °C) and the temperature of metaboric acid formation (130 °C, orthorhombic-III or α-form).[22] After separating the ethanolamine in excess from the reaction media by pouring acetone on the produced gel, a yellowish powder formed, which was then isolated by filtration. The compound could then be dissolved in water up to concentrations of 20% w/v (Fig. S-2, ESI†).

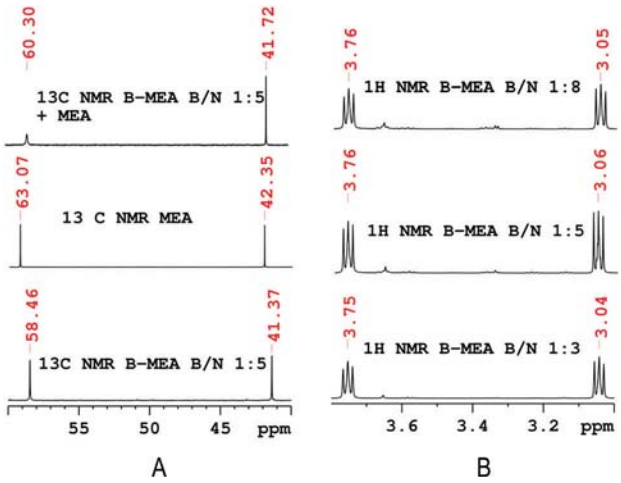

Fig. 1 ^{13}C-NMR spectra of the complexes synthesized by reaction between boric acid and ethanolamine at 1 : 5 stoichiometric ratio in D_2O (B-MEA B/N 1 : 5), ethanolamine, and B-MEA B/N 1 : 5 in the presence of ethanolamine (A). ^{1}H NMR spectra of the complex produced by boric acid and ethanolamine at different stoichiometric ratio (*i.e.* 1 : 3, 1 : 5 and 1 : 8) (B).

We were interested to correlate the molecular architecture in solution with the originated photoluminescence properties (see next section). To this aim, we performed structural analysis by using ^{1}H, ^{13}C, ^{11}B NMR, analytical ultracentrifugation (AUC) and compared our findings with density functional theory (DFT) optimized geometries.

The ^{13}C-NMR spectrum of the complex synthesized by reaction of boric acid and ethanolamine initially present at a stoichiometric ratio 1 : 5 (here abbreviated as B-MEA B/N 1 : 5) (Fig. 1A bottom) shows two peaks located at 58.5 ppm and 41.4 ppm, which can be ascribed to chemical shifts arising from O–$\underline{C}H_2$ and N–$\underline{C}H_2$, respectively. The pure ethanolamine spectrum (Fig. 1A middle) displays these peaks at 63.1 ppm and 42.3 ppm. On the other hand, when pure ethanolamine and the compound of interest (B-MEA B/N 1 : 5) are mixed in D_2O and then analyzed by ^{13}C NMR (Fig. 1A top), the chemical shifts of the two peaks are observed at intermediate values between the two previous spectra (*i.e.* 60.3 ppm and 41.7 ppm). As the change in pH values follow the order: MEA > B-MEA B/N 1 : 5 + MEA > B-MEA B/N 1 : 5, the difference in chemical shift between the three spectra can be attributed to the change in pH occurring upon the introduction of boric acid in the mixture.

Another relevant feature observed on the ^{13}C-NMR peak of the mixture between pure ethanolamine and the compound of interest is the broadening of the peak ascribed to O–$\underline{C}H_2$ at 60.30 ppm compared to the single components (FWHM = 3.1 Hz for B-MEA B/N 1 : 5 and 1.48 Hz for MEA *vs.* 12.5 Hz for the mixture). This is the result of a mixture of ethanolamine molecules whose carbon in the α position with respect to the

oxygen participates in hydrogen bonding with the polyborates (*i.e.* which then affect its chemical shift) and the presence of free ethanolamine in solution.

Another verification that ethanolamine is interacting with the polyborates is the retaining of the ^{1}H compound chemical shifts synthesized at different boric acid/ethanolamine stoichiometric ratios (Fig. 1B). As an increase of ethanolamine generates a variation of the pH and thus a change in the chemical shifts similar to what observed in the ^{13}C-NMR spectra, it indirectly proves that ethanolamine stabilizes the formation of polyborates with well-defined boric acid-ethanolamine ratios.

Only two peaks are visible from the ^{1}H-NMR spectra of the compound dissolved in D_2O. Since hydroxyl and amine groups undergo proton–deuterium exchange, they cannot be detected with the present technique.

The ^{11}B-NMR spectrum of B-MEA helped us to elucidate its molecular architecture. The spectrum is the combination of four different peaks, which can be resolved by deconvolution (Fig. 2). The three broad peaks can be ascribed to tri-coordinate boron ($B_{[3]}$) whereas the narrow peak can be attributed to tetra-coordinate boron ($B_{[4]}$). The difference in peak width arise from different quadrupole coupling constants (QCC).[23]

The appearance of multiple peaks can be correlated to a dynamical equilibrium of various polyborate species upon dispersion in D_2O.[12] Indeed, several studies in literature[24–28] have shown that ^{11}B-NMR analysis of pentaborate species in D_2O solutions yields three characteristic peaks located at 18 ppm, 13 ppm and 1 ppm assigned to monoborate species $B(OH_3)$/$[B(OH)_4^-]$, triborate anions $[B_3O_3(OH_4)^-]$ and pentaborate anions $[B_5O_6(OH)_4^-]$, respectively.

In our case, the four peaks are located at −18.8 ppm, −3.0 ppm, 9.8 ppm and 11.0 ppm. Such shift can be expected as different amine groups were utilized in the above-mentioned studies, (*i.e.* tertiary aliphatics and etheroaromatics[24–28]). By using a primary amine, the Brønsted interaction between the amine ligands and the polyborate is stronger, thus resulting in an upfield of the chemical shift upon complexation with the primary amine ligand if compared with *N*-substituted ones.[10]

The two peaks at 9.8 ppm and 11.0 ppm can then be related to the formation of a dative bond between the primary amine and the trigonal boron atom on the monoborate units, and the acid–base interaction between the tetragonal boric acid and the primary amine[10] on the monoborate units, respectively. By assuming a similar chemical shift as previously observed with triborate and pentaborates, the broad peaks present at −3.0 ppm and −18.8 ppm can be assigned to the acid–base interaction between primary amines[10] and tetragonal boron atoms in the triborate and pentaborate, respectively. The extent of upfield chemical shifts caused by Brønsted interaction with the primary amines is not the same for the monoborate, triborate and pentaborate species (if compared with the single chemical shifts obtained in previous studies[24–28]), probably due to a different solvation degree of the respective polyborates.[29]

Interestingly, the monoborate/triborate/pentaborate ratio found from the deconvolution of the peaks is 24 : 40 : 36, thus the triborate six-membered boroxole ring shows the highest abundance in aqueous solution.

To analyse the size of the complexes formed between ethanolamines and borate, analytical ultracentrifugation (AUC) was performed. Since AUC has a resolution in the Angström range[30] and can distinguish single molecules from their cluster oligomers, it can give a precise idea of the hydrodynamic size of the complexes in the current solution.[31] The measurement showed the presence of species with a size of 0.5 nm, with a negligible concentration of slightly larger species with a size of approximately 3.0 nm (which could be attributed to bigger size complexes not completely cleaved once the product is solubilized in water).[12] To further confirm the results, the solution was also analysed *via* dialysis by using a membrane with pore sizes ranging from 100 to 500 Da. The targeted set of fluorescent compounds passed through the membrane pores, which were calculated to range between 0.3 and 0.5 nm according to the conversion formula: $R_{min} = 0.066 \times M^{1/3}$ between molecular weight and size of biological molecules.[32] Hence, the dialysis experiments already confirmed the results obtained by AUC.

As a mean to investigate the signals obtained by ^{11}B-NMR analysis, the complexes/molecules observed *via* AUC and to elucidate the interactions occurring between polyborates and ethanolamines, DFT calculations were used. Fig. 3 shows the most stable conformations obtained in vacuum from the geometrical optimization of the structures ascribed to the ^{11}B-NMR chemical shifts. In Fig. 3, the diffused bonds between atoms depict hydrogen bonds, which were defined using the geometric criteria published by G. R. Desijaru and T. Steiner.[33] It is clear from Fig. 3a–d that the hydrogen bonds arise mainly from the amine group and the carbon atoms in the backbone chain of the ethanolamine. Following the definition proposed by G. R. Desijaru and T. Steiner,[33] for a bond defined as D–H···A (D = Donor, H = hydrogen, A = acceptor), a hydrogen bond of 'moderate' strength would have a distance between D and A of 2.5–3.2 Å and an angle between 130–180°, while a weak hydrogen bond would be at a distance between 3.0–4.0 Å with an angle ranging from 90° to 180°. Reflecting this on the structures observed during the DFT calculations, it shows that, when N acts as the donor (D) and O as the acceptor (A), the hydrogen bonds observed are of moderate strength, with

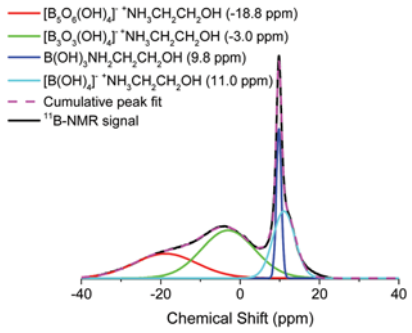

Fig. 2 ^{11}B NMR spectrum deconvolutions (solvent D_2O) of the complex produced by pyrolysis of boric acid and ethanolamine at a 1 : 5 stoichiometric ratio (B-MEA B/N 1 : 5). The deconvolution was obtained by fitting the curve using four Gaussian distributions (R^2 = 0.9984).

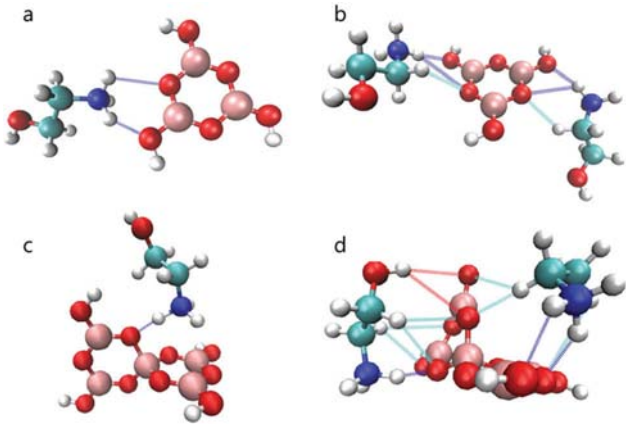

Fig. 3 Geometrical optimization by density functional theory simulations of the fluorophores obtained through the interaction between different polyborates and ethanolamine.

average measured distances of 3.13 Å and average angles of 138.10°. In contrast, when C acts as the donor and O as the acceptor, the average distance found was 3.66 Å and the average angle 132.97°, thus falling in the 'weak' hydrogen bonding classification. When explicit water was added to the system, the hydrogen bonds became slightly weaker. The hydrogen bond lengths increased by 1% to 6% while the angle average values decreased by 2% to 4%. All geometrical measurements are summarized in Tables S1 and S2 (ESI†).

Weak hydrogen bonding associated with the C–OH atom helps explaining the increased peak width in the ^{13}C-NMR peak when both ethanolamines and polyborates are present in solution (Fig. 1A). The broadening of the peak is probably caused by the hydrogen bonds between the N (D) and the O (A) from borates and by the weak interactions involving the C (D) and the O (A). Evidence that the latter interaction increases the stability of the complex arises from comparing the energies of two different configurations obtained when optimizing the geometry of the pentaborate salt with one molecule of ethanolamine, presented in Fig. 3C. The configuration interacting both *via* the amine and the carbons in the backbone was energetically more stable in vacuum compared to the one where the hydrogen bond was solely arising from the amine. The energy difference found was −10.8 kJ mol^{-1}, which is within the range found experimentally for hydrogen bonds.[34] It is well known that C can lead to the formation of hydrogen bonds.[35] These interactions are extremely important in biology where they have an impact on the structure of proteins and nucleic acids, and in enzymatic recognition.[36] For instance, Addlagatta *et al.* showed that in the β-sheets of BPTI the hydrogens were displaced compared to their ideal position to maximise the CH–O bonding potential and thus stabilize the structure.[37] In our case, the formation of multiple interactions between the ethanolamines and the borates in solution, *via* both nitrogen and carbon based hydrogen bonds, helped in stabilizing the complexes.

The DFT calculations can also be used to compare the size of the geometrically optimized complexes to the ones observed *via* AUC. The maximum size was observed for the pentaborate rings complexed with two ethanolamine ligands, with a radius of 0.5 nm, which is in agreement with the AUC results. The weight of this complex was 255 Da, which is below the 300 Da averaged membrane cut-off used during the dialysis experiment and explains why during this experiment all the solutes passed through the membrane.

Optical properties of the polyborates/ethanolamine complexes

The synthesized complexes, besides showing excellent photoluminescence emission in the solid state (Fig. S-4 left, ESI†), also retain fluorescence in solution (Fig. S-4 right, ESI†). Additionally, the complexes show remarkable photostability, with basically no loss on fluorescence signal over 20 h of continuous irradiation. As a simple mixture of monoethanolamine with boric acid does not lead to fluorescence emission, we have concluded that the sole responsibility for the observed fluorescence is a mixture of triborates and pentaborates stabilized by different stoichiometric amounts of ethanolamine through electrostatic interactions and hydrogen bonding.

This mixture of fluorophores (Fig. 3) leads to an excitation-dependent emission profile in solution with the maximum found at 380 nm (Fig. 4).

J. Liang *et al.*[16] have also shown an excitation-dependent fluorescence emission of a complex composed of polyborates and isopropyltrimethylammonium hydroxide. The radiative emission was explained as a consequence of the formation of structural defects in the solid caused by the heating treatment.

Such optical behaviour has also been previously observed in carbon nanodots (CNDs),[38] although in this study the formation of CNDs can be excluded as the complex was not retained by dialysis performed with the lowest cut-off membrane size (*i.e.* 100–500 Da) and AUC results shows a monodisperse size for the amino-polyborates of 5 Å. M. Fu *et al.*[17] mimicked the CNDs excitation-dependent emission behaviour by mixing polycyclic aromatic fluorophores with different fluorescence properties, thus such feature might be the consequence of the heterogeneity in fluorescence emission of different boroxole–amine complexes. However, it cannot be excluded that the insertion of the amine leads to a deformation of the boroxole aromatic ring, causing the formation of self-trapped states, whose band gap vary as a result of the hydrogen bonding strength between MEA and the B–OH motifs.[18]

Moreover, if we consider the UV-Vis absorption profile (Fig. S-5, ESI†), we can determine that, similarly to carbon nanodots, the profile is not specular to the emission pattern, and thus

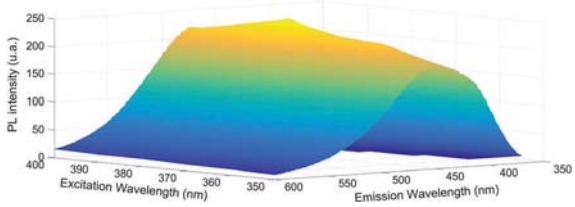

Fig. 4 Excitation-dependent emission of B-MEA B/N 1 : 5.

a different photoluminescence mechanism must be involved when compared to conventional organic fluorophores.

The explanation behind this phenomenon is probably related to the exciton self-trapping or excimer formation. The photoexcited exciton can induce a deformation of the aromatic core, thereby causing a binding between the exciton and the distortion. This would form a polaron, which reduces the exciton bandgap by several millivolts and would allow the emission of radiation in the visible range. Although this effect has already been mimicked for pyrene and perylene,[17] in this study the excimer formation is probably caused by hydrogen bonding between the neighbouring boroxole rings.

Optical glucose sensing *via* aggregation-induced emission (AIE)

As already specified in the previous section, the produced fluorescent complexes between polyborates and amine ligands lead to a set of compounds with outstanding hydrostability.

Due to the presence of B–OH moieties in these complexes, their fluorescence response is expected to change in the presence of 1,2-diols.[7]

Since the aim was to develop a proof of concept for the use of this optical sensor towards monitoring glucose concentrations in wound exudate, all measurements were performed in a phosphate buffer saline (PBS) solution as a model solution (Fig. 5). Although the optical response was tested at different concentrations of B-MEA B : N 1 : 5 as well as three different pH values (*i.e.* 6.2, 6.8, 7.4) (Fig. S-8, ESI†), the kinetic measurements showed the most pronounced increase in fluorescence emission when using a solution of 4 wt% of B-MEA B : N 1 : 5 at a pH of 6.8. The different optical response to glucose at different pH values is a well-known phenomenon related to the pH-dependent formation of boronate esters. This has already been observed in other non-enzymatic glucose sensors and it depends on the acidity constant of the polyborate unit.[39] In addition, in order to expand the sensor operativity range to physiological pH values, the acidity of the boron center was increased *via* the use of a Brønsted type interaction with an amine ligand.[40,41]

In this study, the optical glucose sensor is not only functioning at physiological pH values, but the complex also increases its emission intensity upon the introduction of glucose (Fig. 5A).

This behaviour is divergent from previous literature on non-enzymatic glucose sensing based on fluorophore-induced aggregation of directly linked boronic acid moieties.[39] This conundrum can be explained as a result of aggregation-induced emission (AIE) phenomenon.[42] Hence, the presence of glucose as cross-linker between the polyborate–amine complexes decreases the intramolecular rotation of the boroxole rings (Fig. 3), which in turn increases their fluorescence quantum yield by stabilization of the planar structure. The same AIE behaviour has recently been observed in the presence of graphene carbon dots functionalized with boric acid groups.[43]

The calibration of the optical sensor in the physiological range for glucose (0–8 mM) after stabilization of the signal enhancement provoked by the presence of glucose, can be approximated to a linear fit within the observed glucose concentration range (Adj. R_2 = 0.977) (Fig. 5B).

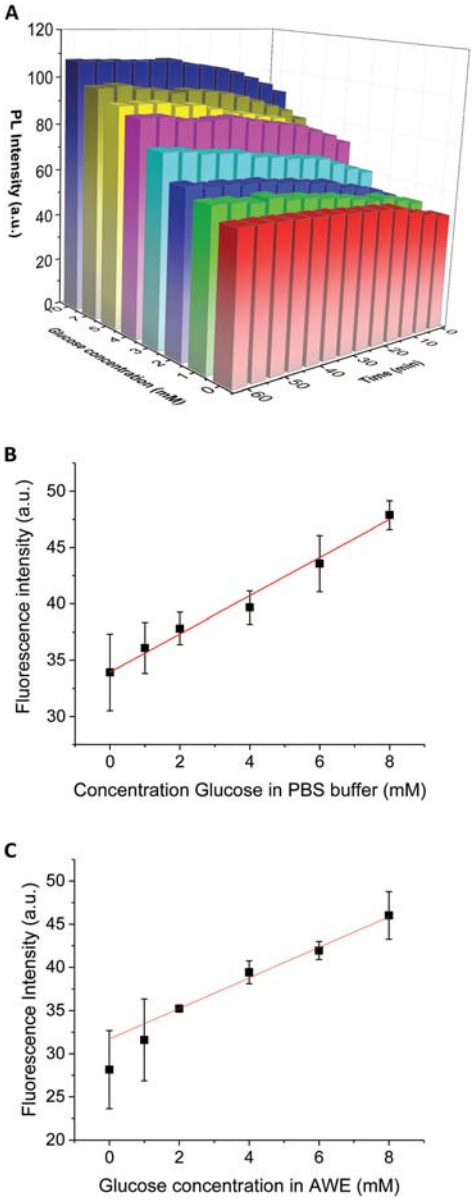

Fig. 5 (A) Fluorescence monitoring of B-MEA B/N 1 : 5 (4 wt%) aggregation-induced emission behaviour in 1× PBS buffer at pH 6.8 at different glucose concentrations; (B) intensity-based calibration of the non-enzymatic optical glucose sensor after 60 minutes contact time (fitting to a linear function: $y = 33.9 + 1.7x$; Adj. R^2 = 0.977); and (C) response of the non-enzymatic optical glucose sensor after 60 minutes contact time in artificial wound exudate, AWE (fitting to a linear function: $y = 31.7 + 1.8x$; Adj. R^2 = 0.978). The fittings in (B) and (C) were performed using a weighted linear regression (which takes the standard deviation of each measurement point into account).

Although the curve can be reasonably fit using a weighted linear regression, multiple binding steps could occur in the presence of polyborates–amine complexes displaying an individual pK_a of cyclic boronate ester formation.

In particular, a fluorescence enhancement of 80% is observed when comparing the signal obtained in the absence of glucose and in the presence of 10 mM glucose.

We have also compared the response of the sensor when working in PBS or artifical wound exudate (AWE, Fig. 5B and C).

Clearly, the presence of exudate components (salts, aminoacids, vitamins, *etc.*) had no effect on the performance of the sensor, both in terms of signal strength, dependence of the signal with glucose concentration, or in the fitting function. Also the kinetics stays the same both in PBS (Fig. 5A) as well as in AWE (Fig. S-9, ESI†). Approximately 40–50 min are needed for a stabilization of the sensor response. We attribute this delay to the AIE behaviour: glucose needs to diffuse to and combine with the B-MEA complexes to induce their crosslinking. This phenomenon, even in solution, requires time to be completed, although agitation of the mixture could contribute to a minimization of the response time. Moreover, we would like to stress that even in the absence of glucose the sensor requires 30–35 min for stabilization, due to conformational changes caused by the solvation of the ethanolamine–polyborate complexes.

In conclusion, the present sensor could be used to reliably assess the concentration of glucose in wound exudates (*e.g.* 0–10 mM).

Granting that the present sensor is not selective towards glucose (see Fig. S-10, ESI†), it is important to notice that potentially interfering species displaying 1,2-diols are present in the wound exudate at negligible concentrations if compared to the observed glucose range.[44–47] Thus, they should not affect the reliability of the glucose sensor. Moreover, we would like to highlight that the sensitivity to specific 1,2-diols could be steered in future works by manipulating the molecular design of the amino ligand.

Although many non-enzymatic optical glucose sensors are already described in literature,[39] this study presents the first example of a complex based on boric acid and an amine ligand as precursors. As this work is presented as proof of concept, this work is expected to pioneer the use of fluorescent amine-polyborate complexes as non-enzymatic optical glucose sensors. Development of fluorescent complexes from cost-effective precursors will increase the viability of these sensors for large-scale applications, such as wound monitoring assessment.

Experimental

Materials

Boric acid, ethanolamine and glucose anhydrous were purchased from Sigma-Aldrich and used without any further purification. Fructose and lactose monohydrate were purchased from Fluka. Phosphate saline buffer (PBS) at different concentrations were prepared by dissolving the desired amount of sodium chloride (Sigma-Aldrich, 99%), potassium chloride (Sigma-Aldrich, 99%), sodium phosphate dibasic (Sigma-Aldrich, 99.95%), potassium phosphate monobasic (Sigma-Aldrich, 99%) in de-ionized water. The pH value was adjusted by using determined amount of NaOH or HCl. Artificial wound exudate (AWE) was prepared as mentioned previously:[21] AWE = DMEM 5030 (Sigma Aldrich) solubilized in PBS buffer (pH 6.2, 6.8 or 7.4), including 10% (v/v) porcine serum (Gibco, Life Technologies).

Synthesis and purification of polyborates/ethanolamine complex

Different amounts of boric acid were introduced into a 100 ml round-bottomed flask (1.93 g, 3.09 g and 5.10 g, related to a stoichiometric ratio with ethanolamine equal to 1 : 3, 1 : 5 and 1 : 8, respectively). Afterwards, 15.27 g of ethanolamine were poured into the reaction vessel and the solution was agitated at 500 rpm with a magnetic stirrer and heated up to 150 °C. After 230 minutes of reaction, a condensed viscous product is collected at the bottom of the flask. Upon addition of 75 ml of acetone, the consistence of the mixture changes from a viscous gel to a powdery slurry. After filtration with sintered disc filter funnel (10–16 μm max. pore size), a yellowish powder is collected on the filter. The precipitate was then transferred with a spatula into a 20 ml glass vial and dried at room temperature under vacuum for 24 h to eliminate the residual ethanolamine.

Optical response to glucose concentration

Optical glucose assays were performed at room temperature on a fluorescence plate reader (Varian, Cary Eclipse). Different concentrations of B-MEA (2, 4 and 6 wt%), PBS buffers or AWE solutions at four pH values (6.2, 6.8, 7.4 and 7.8) as well as different glucose concentrations ranging from 0 to 10 mM were tested to optimize and calibrate the sensor response (λ_{ex} = 380 nm, λ_{em} = 465 nm). The fluorescent signal was collected for all samples with 5 min time points up to a maximum time of 60 min. A similar protocol was used to determine the optical response to fructose and lactose. In these cases, only PBS, pH 6.8, and B-MEA concentration of 4% were used.

Characterization

^{1}H, ^{11}B and ^{13}C NMR spectra were obtained at 298 K on a Bruker Avance 400 (at 400.1, 160.1 and 100.6 MHz, respectively). All measures were performed at 298 K using a 5 mm BBI inverse probe equipped with z-gradient. All spectra were recorded with the Bruker standard pulse programs and parameter sets and the ^{1}H chemical shifts were referenced internally using the resonance signals of D_2O at 4.80 ppm.

Optical characterization of B-MEA was performed with a Cary Eclipse Fluorescence Spectrophotometer equipped with a multiwall-plate reader (Varian). 200 μl of the B-MEA solution at 4% w/v were deposited on a 96 well-plate and analysed at different excitation wavelengths. Photostability measurements were performed with the same fluorescence reader (Varian, Cary Eclipse) under the following conditions: λ_{ex} = 380 nm, λ_{em} = 465 nm, pulse frequency of 80 Hz, source power of 60 kW, 600 min irradiation time with pulse cycles of 0.01 min, medium detector (600 V). UV-Vis spectra were obtained using Varian Cary 50 Bio UV-visible spectrophotometer (open quartz cuvette with an optical path 1 cm).

Analytical centrifugation was used to detect the presence of solutes and analyse their size. The solid was dissolved in water at a concentration of 12 mg ml^{-1}. The samples were sampled using Rayleigh interference optics at 25 °C and 60k rpm. The experiment lasted 18 hours. The data were fitted to the Lamm equation with a non-interacting discrete species model using the software Sedfit Vers. 14.4d.

Computational methods

The density functional theory calculations were performed using CP2K.[48] To perform the DFT based geometry optimization, Quickstep was used. This method, developed by Van de Vondele *et al.*,[49] uses a mixed Gaussian and plane waves approach to calculate the electronic properties of the atoms present in the system. For the exchange correlation function, the Perdew–Burke–Enzerhof method was selected and was used in combination with the corresponding pseudo potentials. All the atoms present in the simulation, apart from the boron, were described using the MOLOPT triple-zeta diffused basis set with polarization.[50] This was chosen to ensure that the electrons on charged atoms would be described in the correct way. The boron was described using a double-zeta diffused basis set, again including polarization. Dispersion forces were added by using the Grimme method.[51] Geometry optimization calculations were run both in vacuum and with explicit water in the first coordination shell of the amine and the central boron of the metaboric acid. Outside this region (10 Å), an implicit water model with a dielectric constant of 78.2 was employed by using the self-correlation reaction field. The plane wave density cut-off was 300 Ry.

Conclusions

In this study, we have demonstrated for the first time that a facile complex formation between polyborates occurring at high temperatures with ethanolamine ligands leads to a one-pot, cost-efficient, up-scalable synthesis of optical glucose sensors. The sub-nm size range of these set of compounds, as determined by molecular dynamics calculation and analytical ultracentrifugation, as well as their carbon dots-like emission properties, render them particularly appealing for the development of optical glucose sensors.

The peculiar increase in emission upon glucose binding has been explained as a consequence of aggregation-induced emission (AIE).

In conclusion, we pioneer a new synthetic route to develop non-enzymatic optical glucose sensors. Future efforts will be directed at steering the selectivity of the resulting sensor by varying the steric hindrance of the amino ligand.

Conflicts of interest

There are no conflicts to declare.

Acknowledgements

This work was supported by a grant from the Swiss Confederation and funded by Nano-Tera.ch within the Nano-Tera project ''Fabrication of fluorescence biosensors in a textile dressing'' for non-invasive lifetime imaging-based wound monitoring', FLUSITEX (RTD2013) that was scientifically evaluated by SNSF. The authors would also like to thank Dr D. Rentsch for his valuable contribution in performing the NMR measurements. We also thank Dr A. Osypova, T. Ramsauer and L. Knezevic for performing some of the B-MEA characterization as well as optical glucose sensing experiments, and R. Rosenberg for performing the AUC experiments.

Notes and references

1 B. T. Koo, W. R. Dichtel and P. Clancy, *J. Mater. Chem.*, 2012, **22**, 17460.
2 B. Lukose, A. Kuc and T. Heine, *Chem. – Eur. J.*, 2011, **17**, 2388–2392.
3 S. S. Han, H. Furukawa, O. M. Yaghi and W. A. Goddard, *J. Am. Chem. Soc.*, 2008, **130**, 11580–11581.
4 H. Yang, H. Wu, F. Pan, Z. Li, H. Ding, G. Liu, Z. Jiang, P. Zhang, X. Cao and B. Wang, *J. Membr. Sci.*, 2016, **520**, 583–595.
5 S.-Y. Ding, J. Gao, Q. Wang, Y. Zhang, W.-G. Song, C.-Y. Su and W. Wang, *J. Am. Chem. Soc.*, 2011, **133**, 19816–19822.
6 M. Dogru and T. Bein, *Chem. Commun.*, 2014, **50**, 5531–5546.
7 R. Nishiyabu, Y. Kubo, T. D. James and J. S. Fossey, *Chem. Commun.*, 2011, **47**, 1124–1150.
8 J. L. Segura, M. J. Mancheño and F. Zamora, *Chem. Soc. Rev.*, 2016, **45**, 5635–5671.
9 Y. Du, K. Mao, P. Kamakoti, P. Ravikovitch, C. Paur, S. Cundy, Q. Li and D. Calabro, *Chem. Commun.*, 2012, **48**, 4606–4608.
10 Y. Du, K. Mao, P. Kamakoti, B. Wooler, S. Cundy, Q. Li, P. Ravikovitch and D. Calabro, *J. Mater. Chem. A*, 2013, **1**, 13171–13178.
11 Y. Du, D. Calabro, B. Wooler, P. Kortunov, Q. Li, S. Cundy and K. Mao, *Chem. Mater.*, 2015, **27**, 1445–1447.
12 M. A. Beckett, *Coord. Chem. Rev.*, 2016, **323**, 2–14.
13 M. S. Wang, G. C. Guo, W. T. Chen, G. Xu, W. W. Zhou, K. J. Wu and J. S. Huang, *Angew. Chem., Int. Ed.*, 2007, **46**, 3909–3911.
14 M. C. Liu, P. Zhou, H. G. Yao, S. H. Ji, R. C. Zhang, M. Ji and Y. L. An, *Eur. J. Inorg. Chem.*, 2009, 4622–4624.
15 Y. Yang, J. B. Sun, M. Cui, R. Bin Liu, Y. Wang and C. G. Meng, *J. Solid State Chem.*, 2011, **184**, 1666–1670.
16 J. Liang, Y. G. Wang, Y. X. Wang, F. H. Liao and J. H. Lin, *J. Solid State Chem.*, 2013, **200**, 99–104.
17 M. Fu, F. Ehrat, Y. Wang, K. Z. Milowska, C. Reckmeier, A. L. Rogach, J. K. Stolarczyk, A. S. Urban and J. Feldmann, *Nano Lett.*, 2015, **15**, 6030–6035.
18 S. Wang, I. S. Cole, D. Zhao and Q. Li, *Nanoscale*, 2016, **8**, 7449–7458.
19 X. Sun and T. D. James, *Chem. Rev.*, 2015, **115**, 8001–8037.
20 V. L. Alexeev, S. Das, D. N. Finegold and S. A. Asher, *Clin. Chem.*, 2004, **50**, 2353–2360.
21 D. A. Jankowska, M. B. Bannwarth, C. Schulenburg, G. Faccio, K. Maniura-Weber, R. M. Rossi, L. Scherer, M. Richter and L. F. Boesel, *Biosens. Bioelectron.*, 2017, **87**, 312–319.
22 D. Schubert, *Kirk-Othmer Encyclopedia of Chemical Technology*, John Wiley & Sons, Inc., 2000.

23 N. Feng, A. Zheng, Q. Wang, P. Ren, X. Gao, S. Bin Liu, Z. Shen, T. Chen and F. Deng, *J. Phys. Chem. C*, 2011, **115**, 2709–2719.
24 M. A. Beckett, P. N. Horton, M. B. Hursthouse and J. L. Timmis, *RSC Adv.*, 2013, **3**, 15185–15191.
25 M. A. Beckett, P. N. Horton, M. B. Hursthouse and J. L. Timmis, *Polyhedron*, 2014, **77**, 96–102.
26 M. A. Beckett, C. C. Bland, P. N. Horton, M. B. Hursthouse and K. S. Varma, *J. Organomet. Chem.*, 2007, **692**, 2832–2838.
27 M. A. Beckett, S. J. Coles, R. A. Davies, P. N. Horton and C. L. Jones, *Dalton Trans.*, 2015, **44**, 7032–7040.
28 M. A. Beckett, C. C. Bland and K. Sukumar Varma, *Polyhedron*, 2008, **27**, 2226–2230.
29 L. Zhu, S. H. Shabbir, M. Gray, V. M. Lynch, S. Sorey and E. V. Anslyn, *J. Am. Chem. Soc.*, 2006, **128**, 1222–1232.
30 H. Cölfen and T. Pauck, *Colloid Polym. Sci.*, 1997, **275**, 175–180.
31 M. Kellermeier, R. Rosenberg, A. Moise, U. Anders, M. Przybylski and H. Colfen, *Faraday Discuss.*, 2012, **159**, 23–45.
32 H. P. Erickson, *Biol. Proced. Online*, 2009, **11**, 32–51.
33 G. R. Desiraju and T. Steiner, *The Weak Hydrogen Bond*, 1999, vol. 9.
34 D. T. Haynie, *Biological Thermodynamics*, Cambridge University Press, Cambridge, 2nd edn, 2008.
35 T. Steiner and G. R. Desiraju, *Chem. Commun.*, 1998, 891–892.
36 S. Horowitz and R. C. Trievel, *J. Biol. Chem.*, 2012, **287**, 41576–41582.
37 A. Addlagatta, S. Krzywda, H. Czapinska, J. Otlewski and M. Jaskolski, *Acta Crystallogr., Sect. D: Biol. Crystallogr.*, 2001, **57**, 649–663.
38 C.-P. Hsu, Z. Hejazi, E. Armagan, S. Zhao, M. Schmid, H. Zhang, H. Guo, L. Weidenbacher, R. M. Rossi, M. M. Koebel, L. F. Boesel and C. Toncelli, *Sens. Actuators, B*, 2017, **253**, 714–722.
39 X. Wu, Z. Li, X.-X. Chen, J. S. Fossey, T. D. James and Y.-B. Jiang, *Chem. Soc. Rev.*, 2013, **42**, 8032.
40 J. D. Larkin, J. S. Fossey, T. D. James, B. R. Brooks and C. W. Bock, *J. Phys. Chem. A*, 2010, **114**, 12531–12539.
41 T. D. James, K. R. A. S. Sandanayake, R. Iguchi and S. Shinkai, *J. Am. Chem. Soc.*, 1995, **117**, 8982–8987.
42 Y. Hong, J. W. Y. Lam and B. Z. Tang, *Chem. Soc. Rev.*, 2011, **40**, 5361.
43 L. Zhang, Z.-Y. Zhang, R.-P. Liang, Y.-H. Li and J.-D. Qiu, *Anal. Chem.*, 2014, **86**, 4423–4430.
44 I. A. Buchan, J. K. Andrews, S. M. Lang, J. G. Boorman, J. V. Harvey Kemble and B. G. H. Lamberty, *Burns*, 1981, **7**, 326–334.
45 K. F. Cutting, *Br. J. Community Nurs.*, 2003, **8**, S4–S9.
46 I. A. Buchan, J. K. Andrews and S. M. Lang, *Burns*, 1981, **8**, 39–46.
47 N. J. Trengove, S. R. Langton and M. C. Stacey, *Wound Repair Regen.*, 1996, **4**, 234–239.
48 CP2K developers group, *CP2K version 4.0 (Development Version)*, 2015. CP2K is freely available from http://www.cp2k.org/ (accessed January 2017).
49 J. Vandevondele, M. Krack, F. Mohamed, M. Parrinello, T. Chassaing and J. Hutter, *Comput. Phys. Commun.*, 2005, **167**, 103–128.
50 J. VandeVondele and J. Hutter, *J. Chem. Phys.*, 2007, **127**, 114105.
51 S. Grimme, J. Antony, S. Ehrlich and H. Krieg, *J. Chem. Phys.*, 2010, **132**, 154104.